JOURNAL OF PROPULSION AND POWER
Vol. 25, No. 1, January–February 2009

Oscillatory Flows of Rectangular Hypersonic Inlet Unstart Caused by Downstream Mass-Flow Choking

Hui-jun Tan* and Shu Sun†
Nanjing University of Aeronautics and Astronautics, 210016 Nanjing, People's Republic of China
and
Zhi-long Yin‡
Hongdu Aviation Industry Group, 330024 Nanchang, People's Republic of China

DOI: 10.2514/1.37914

Unstart flows of a rectangular hypersonic inlet are experimentally studied at a freestream Mach number of 5. With the aid of high speed Schlieren and time-accurate pressure measurements, the unsteady flow processes of the entire inlet, including the shock system motions, the separation bubble transformations, and the surface pressure fluctuations, are recorded and discussed. The relation of the oscillation frequency with the exit throttling ratio is also obtained. Results indicate that the oscillatory flows of hypersonic inlet unstart can be classified into two types, namely, relatively mild "little buzz" and highly violent "big buzz." Because of the presence of a large transient supersonic region in the duct, the upstream propagation of acoustic waves is impeded temporarily in a buzz cycle. As a result, the traditional oscillation mechanism of supersonic inlet buzz, based on an acoustic wave feedback loop, is invalid for hypersonic inlet buzz. Therefore, a new oscillation mechanism is brought forward in which the airflow spillage at the entrance of the inlet is taken as the disturbing source and three communicating ways, namely, convection, shock train motion, and acoustic wave propagation, jointly establish the signal feedback loop. Then, the base frequencies of hypersonic inlet buzz at different throttling ratios are estimated and found in good consistency with those observed in current experiments.

I. Introduction

A HYPERSONIC inlet is an important component of hypersonic airbreathing engines. Being capable of starting and restarting at any Mach number in the flight envelope is a basic requirement of hypersonic inlets for proper and efficient operations. In principle, the unstart phenomenon of hypersonic inlets should always be avoided. But due to the immaturity of design methods, the inaccuracy of computational fluid dynamics tools, the inconsistency of ground simulated conditions with flight conditions, and the uncertainty of engine thrust regulations, the unstarted conditions of hypersonic inlets occur inevitably during the development of hypersonic airbreathing propulsion systems. In the joint scramjet flight test of the Central Institute of Aviation Motors and NASA, which was carried out in 1998, unstart of the hypersonic inlet led to a partial unfulfillment of the scheduled flight task [1]. According to the subsequent analysis made by Voland et al., the inlet started at a Mach number of 3.5, but soon unstarted due to overfueling of the combustor and remained unstarted till the flight Mach number reached 5.0. The inlet unstarted condition lasted 12 s during the flight test.

In general, when the airflow capture characteristic of a hypersonic inlet is not affected by the change of the internal flowfield, it is regarded as operating in a started mode, otherwise in an unstarted condition [2]. Unstart of a hypersonic inlet can result either from design factors (such as large internal area-contract ratios, serious shock/boundary layer interactions, etc.) or from using factors (such as low flight Mach number, large angle of attack, high backpressure, etc.). While unstarted, hypersonic inlets usually suffer from violent shock system oscillations, prominent pressure fluctuations, and abrupt performance reductions which results in a substantial engine thrust loss and even the combustor flameout [3,4]. Furthermore, the caused unsteady aerodynamic loads are highly detrimental to the structural safety of scramjets and the flight control of vehicles. Therefore, we are in urgent need of a comprehensive understanding in hypersonic inlet unstart to fulfill the future tasks: 1) provide unsteady flow patterns and base frequency characteristics for the detection and prediction of hypersonic inlet unstart, and also for the structural strength design of scramjets and vehicles, 2) reveal the oscillation mechanism of hypersonic inlet buzz and establish the prediction method for oscillation frequency, and 3) explore the suppression method for hypersonic inlet buzz.

II. Literature Review

Since Oswatitsch's first observation of the oscillatory aerodynamic phenomenon (known as buzz) of supersonic inlets [5], much work has been devoted to this special subject for its description, prediction, and suppression. Ferri and Nucci [6] and Dailey [7] performed the foundational work on the physical mechanism of supersonic inlet buzz, individually putting forward two different criteria which are based on strong shear layer theory and shock-induced separation theory. The succeeding numerical and experimental investigations made by Fisher et al. [8], Sajben et al. [9], Newsome [10], Lu and Jain [11], Trapier et al. [12], etc. improved the understanding of buzz flows further. For supersonic inlet buzz there exist two different instability phases of similar frequencies but of different amplitudes, called "little buzz" and "big buzz." As inlet buzz is a self-excited flow essentially, it is generally agreed that there exists a feedback loop of signals in which the acoustic wave often plays the role of upstream feedback. Therefore, the base frequency and other energy-containing frequencies are often closely related to the acoustic resonant modes of the duct. In 2007, Trapier et al. [13] and Hirschen et al. [14] attempted to detect and predict the onset of supersonic inlet buzz by transient signal analysis. They also tried to suppress the oscillation amplitudes by means of boundary layer bleeding.

But Curran and Murthy [2] point out that for hypersonic inlets the unstarted flow pattern is quite different from that of supersonic inlets. Achievements in supersonic inlet buzz cannot be applied to

Received 6 April 2008; revision received 30 August 2008; accepted for publication 19 September 2008.

*Professor, College of Energy and Power Engineering.
†Associate Professor, College of Civil Aviation.
‡Engineer, 660 Institute.

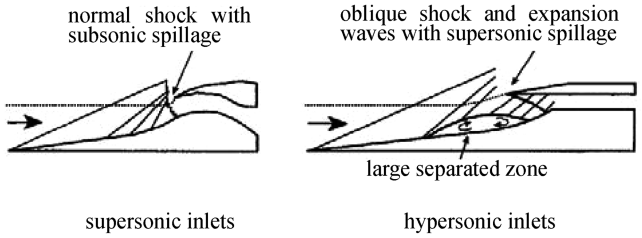

Fig. 1 Flow patterns of mixed-compression inlets at unstarted conditions [2].

hypersonic inlets directly. For example, the expelled shock system of hypersonic inlets does not contain a normal shock similar to supersonic inlets. As a result, the airflow is spilled supersonically for hypersonic inlets but subsonically for supersonic inlets (Fig. 1). Therefore, extra work was done to reveal the flow patterns of unstarted hypersonic inlets as reported by Scott [15], Bao et al. [16], Yuan and Liang [17], and Sun et al. [18]. Some useful conclusions were drawn; however, the authors dealt with the unstart phenomenon mainly in a steady manner which blurred its oscillatory nature, diminished its possible threat, and provided an unreliable basis for its detection and prediction. In [19], the mean and time-accurate pressures in a two-dimensional hypersonic inlet were measured both under backpressure-induced unstart conditions and under cowl-induced unstart conditions. The unsteadiness of hypersonic inlet unstarted flow was noticed, but due to the insufficiency of dynamic pressure gauges and the lack of flow visualization, the unsteady flow patterns of hypersonic inlets were still obscure. What is worse, in some cases even the authors of [19] were not sure whether the observed unsteady pressure behaviors were the result of noisy measurements or not. Tan and Guo [4] investigated the unsteady flows of an unstarted 3-D hypersonic inlet for dual-combustor ramjets. Violent oscillations of the external shock system and surface pressures were observed in their experiment. However, due to the geometric complexity of the internal duct and the inadequate resolution of the shadowgraph images, Tan and Guo failed to depict typical flow patterns of a buzz cycle, and a majority of their conclusions were inferred according to the instantaneous surface pressures. To sum up, the differences between hypersonic inlet buzz and supersonic inlet buzz in unsteady flow patterns, oscillatory characteristics, and oscillation mechanisms are still left unknown.

III. Description of the Test Model

As shown in Fig. 2, the test model, which simulates the full flowpath of a generic rectangular scramjet engine, consists of an inlet, an isolator, a dump combustor, and a flow plug. The inlet has a maximum capture area of 67.5×70 mm^2 and is designed for a shock-on-lip Mach number of 6.0 and for a starting Mach number of 4.0. The external compression of the inlet is achieved by two ramps inclined by 10 and 21 deg to the freestream flow direction, respectively. The flow turning angle at the internal cowl is 13 deg. The total area contraction ratio of the inlet is 6.4 and the internal one is 2.2. To avoid the interference of the expansion waves originating from the side edges of the forebody, the width of the forebody decreases along the flow direction with a converging angle of local Mach cone angle at a free Mach number of 4.0. Immediately after the inlet throat, a constant cross-sectional duct (100 mm in length and 10.5 mm in height) lies and acts as the isolator. Downstream of the

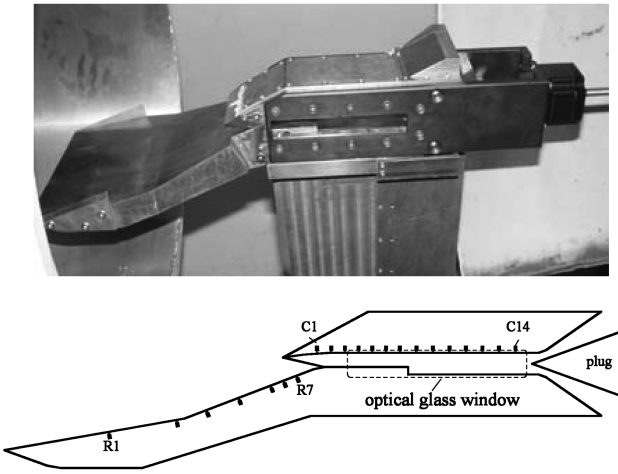

Fig. 2 The test model.

isolator is a simplified dump combustor with a length of 90 mm and a height of 16 mm. Two pieces of K9 glass (130 mm in length and 20 mm in height) are installed on the two sides of the duct, providing optical access to the internal flowfield. At the duct exit, a flow plug with a wedge angle of 40 deg, driven by a linear electric motor, is placed to obtain the combustion induced high pressure. The inlet operating conditions can be varied by changing the axial position of the flow plug which is identified by the throttling ratio (TR):

$$\mathrm{TR} = (1 - A_{\mathrm{th,plug}}/A_{\mathrm{combustor}}) \times 100\%$$

where $A_{\mathrm{th,plug}}$ is the throat area near the plug and $A_{\mathrm{combustor}}$ is the cross-sectional area of the combustor. During each test, TR can be set to any value between 0% (fully opened) to 100% (fully closed).

IV. Experimental Conditions and Measurements

These experiments are conducted in the hypersonic wind tunnel of Nanjing University of Aeronautics and Astronautics. The facility runs in a blown-down mode with a usable run time greater than 7 s. The test chamber is fully closed with two embedded glass windows (300 mm in diameter) for optical access. Upstream of the test chamber an interchangeable converging–diverging nozzle with an exit diameter of 500 mm is located, providing nominal freestream Mach numbers from 5.0 to 8.0 and flight conditions from 27 to 59 km. For current experiments, the Mach 5 nozzle is used and the corresponding flow conditions are summarized in Table 1 [20].

Time-accurate pressure measurements are performed by 21 dynamic pressure transducers to monitor the unsteady flow patterns of the inlet. The transducers are labeled by R1–R7 (R1–R5: range of 100 kPa; R6–R7: range of 500 kPa) and C1–C14 (range of 500 kPa) in Fig. 2. These transducers have an accuracy of $\pm 0.1\%$ of the full range and a natural response frequency of 50 kHz. Obviously, the internal cavum of the transducer and the conduit degrade the actual frequency response. For current tests, the volume of the cavum is 40 mm^3 and the longest conduit does not exceed 40 mm. Thus, according to a conservative estimate [4], the cutoff frequency of the pressure system is higher than 1714 Hz, taking the speed of sound as 300 m/s. The data acquisition system consists of two National Instruments DAQ PCI-6115 cards. During tests, the data sampling

Table 1 Test conditions for hypersonic inlet unstart

Property	Value
Nominal Mach no.	5.0
Actual Mach no.	4.92
Total temperature, K	580
Total pressure, 10^6 Pa	0.6–0.7
Usable run time, s	>7
Diameter of the uniform flow region at the station of 300 mm downstream of the nozzle exit, mm	>300

frequency is set to 20 kHz per channel and the sampling process lasts for 10 s to cover the entire operating process of the wind tunnel. In general, the cutoff frequency of the pressure system should be 3 times the interested frequency or higher; thus the effective bandwidth is 570 Hz for all analyses presented in this paper.

The unsteady behaviors of the external and internal flows are also recorded by a CR2000 camera of Kodak, Inc. The sampling rate of the Schlieren visualization can reach as high as 2000 frames per second, but the corresponding sampling process lasts for just 1 s due to the memory limit. Therefore, the high speed camera is triggered manually with an external pulse signal after the establishment of the flowfield in the test chamber. The triggering signal is also recorded by the data acquisition system to obtain synchronization between two measurement systems.

V. Started Flows

Before plunging into the unstarted conditions, it is worthwhile to discuss the started flowfield first. For the present hypersonic inlet, stable-started conditions can be obtained for TRs less than 50% at a freestream Mach number of 4.92. While TR equals 0%, the inlet operates at a free backpressure condition. While TR equals 38.4%, the duct exit is slightly blocked and the inlet operates at a high backpressure condition. Figures 3 and 4, in which the boundary of the flow region and the transducers are outlined with white solid lines, portray typical started flow patterns of the inlet. As can be seen, the internal flow structure of the inlet is rather complex, including the generation, reflection and intersection of shock waves and expansion waves, and the interaction of shock waves and boundary layers or free shear layers. Quite different from that of external compression supersonic inlets, the external shock system of the hypersonic inlet does not contain a normal shock. Furthermore, at a high backpressure the terminal shock system of the hypersonic inlet takes the form of a complex and asymmetric shock train rather than a normal shock.

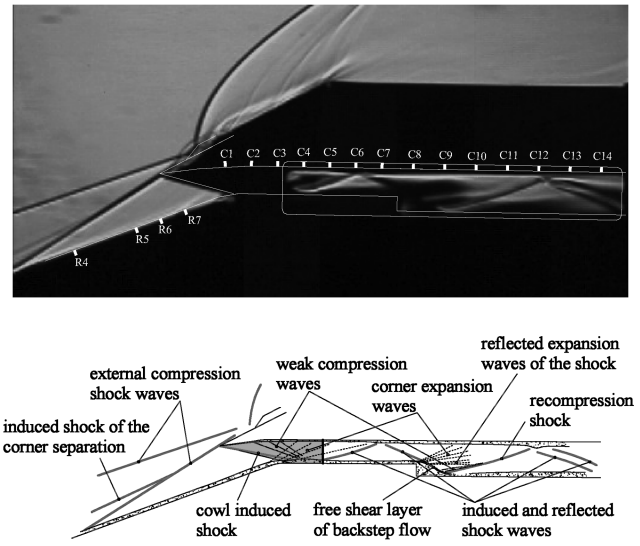

Fig. 3 Flow pattern of the inlet while the duct exit is fully opened (TR = 0%).

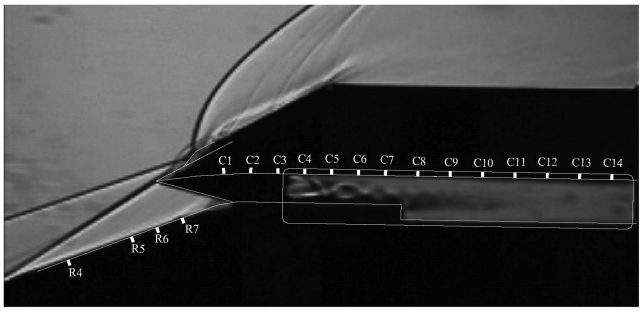

Fig. 4 Flow pattern of the inlet while the duct exit is slightly blocked (TR = 38.4%).

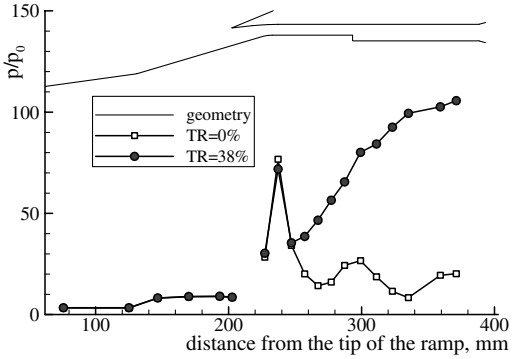

Fig. 5 Distributions of the time-averaged surface pressures of the started hypersonic inlet.

To aid in understanding the started inlet flows at different TRs, Fig. 5 exhibits the distributions of the time-averaged surface pressures. The integral time is chosen as 3 s and the static pressures are normalized by the freestream static pressure. The values of R7 and C12 survey points are blanked due to the transducer damage in the experiment. Noticeably, along the streamwise direction the surface pressures are distributed evenly on each ramp and an abrupt increase exists near the ramp corner. While TR equals 0%, due to the reflections of shock waves and expansion waves, the surface pressure distribution of the internal cowl undulates along the flow direction and most of the pressure values keep below 35 times the freestream pressure. As TR is raised to 38.4%, the shock train in the isolator forces the wall static pressure after the C3 survey point to climb up continuously to 106 times the freestream pressure (at the C14 survey point).

As to the flow steadiness, the surface pressures of the entire inlet are fairly stable at a TR of 0% according to the time-resolved pressure histories, but at a TR of 38.4% the surface pressures of the isolator exhibit an oscillatory feature due to the emergence of the shock train. Taking the example for the C5 survey point, the rms value of the static pressure remains below one-fifth of the freestream pressure at a TR of 0%, but at a TR of 38.4% the value reaches as high as 4 times the freestream pressure. Schlieren visualizations also confirm the time-accurate measurements of surface pressure. At a TR of 0%, no perceptible unsteadiness of the flow pattern can be noticed according to the Schlieren movie. While at a TR of 38.4%, the shock train at the isolator oscillates streamwisely with a scope of one-fourth of the isolator height.

VI. Oscillatory Unstarted Flows

When the throttling ratio is increased to or above 50%, transient airflow spillage occurs according to the analysis of Schlieren movies. In other words, hypersonic inlet unstart appears. The unstarted flow patterns observed in current experiments, which all demonstrate substantial unsteadiness, can be classified into two distinct types, namely, a relatively mild type and a highly violent type. Borrowing terms from supersonic inlet buzz descriptions, the mild one is called little buzz and the violent one is called big buzz in this paper.

A. Little Buzz Flow (TR = 50%)

Schlieren pictures show that while TR is increased to 50%, the internal shock train is pushed to the contracting part of the inlet, resulting in a large separation bubble near the ramp side and a strong induced oblique shock (Fig. 6). The separation bubble narrows the effective passage of the isolator and the induced oblique shock decreases the upstream Mach number of the shock train. Therefore the shock train is substantially shortened. Actually, the entire internal flow in the visible area exhibits subsonic flow features. The separation induced shock also causes an abrupt rise of local pressure which leads to airflow spillage at two sides of the duct entrance.

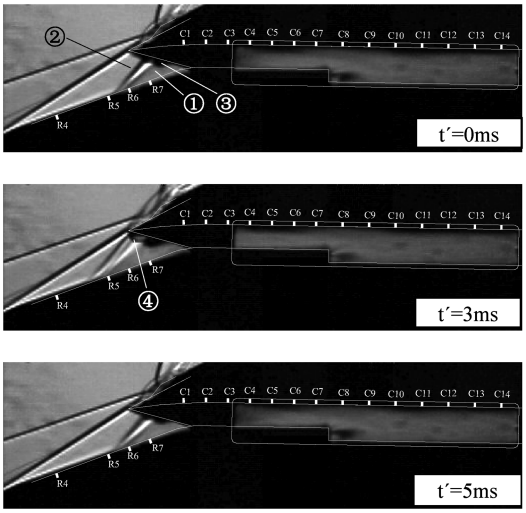

① separation bubble; ② separation bubble induced oblique shock;

③ the reflected expansion waves of the cowl originated shock on the boundary of the separation bubble;

④ the detached cowl shock.

Fig. 6 Typical Schlieren pictures in a little buzz cycle (TR = 50%).

Further analysis of the time-resolved Schlieren movie indicates that the entrance separation bubble shrinks and expands in a 5 ms cycle and with a bubble height fluctuating from 6 to 8 mm. Also the tip point of the separation bubble oscillates along the flow direction with a scope of 11 mm, resulting in the periodical motion of the induced oblique shock. While the oblique shock is at its most upstream position (Fig. 6, $t' = 3$ ms), it impinges around the cowl tip, and the cowl originated shock is detached due to the decreased upstream Mach number (about 2.0) and the increased flow turning angle (about 30 deg). Transient airflow spillage is thus formed above the cowl. Therefore, the inlet operating state at a TR of 50% is called unstart due to the change in airflow capture characteristics.

Static pressure-time histories of typical survey points during little buzz are exhibited in Fig. 7 from which one can notice that the unsteady behaviors of the separation bubble and the induced oblique shock lead to periodical variations of the internal surface pressures. The pressure fluctuation of C01 is the highest among all survey points and approximates 30 times the freestream pressure. Also, the pressure fluctuation of R05 is fairly high because the foot of the separation induced shock happens to sweep it frequently. The power spectrum density calculations of C01 and R05 show that the fluctuating energy is mainly contained in the frequency region below 500 Hz (Fig. 8). Multiple peak frequencies can be observed in Fig. 8 and the two most prominent peaks are round 190 and 234 Hz, respectively. The acoustic resonance frequencies of the test model can be estimated by the following formula which is used for predicting resonance modes of a duct with an open end and a closed end in [10]:

$$f_n = (2n+1)\frac{c}{4L}(1-M^2) \qquad n = 0, 1, 2, \ldots$$

where L is the length of the duct, c the speed of sound, and M the Mach number of the flow along the duct. According to the present experiment, L represents the distance between the cowl lip (the open end) and the throat near the exit plug (acting acoustically like a closed end) and equals 0.19 m. M should be the average Mach number of the isolator/combustor and can be estimated according to the mass-flow continuity constraint. Supposing that the throat near the exit plug is always choked and that the total pressure loss of the subsonic flow in the combustor can be neglected, one obtains $M = 0.4$, $C = 461$ m/s, and $f_0 = 510$ Hz. The fundamental acoustic resonance frequency of the duct is obviously higher than any peak frequency marked in Fig. 8. Therefore, it can be inferred that

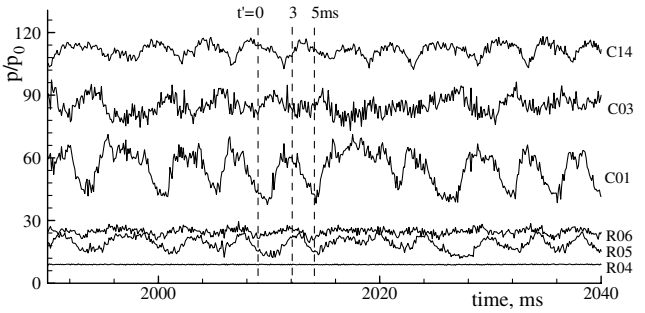

Fig. 7 Static pressure-time histories of typical survey points during a little buzz (TR = 50%).

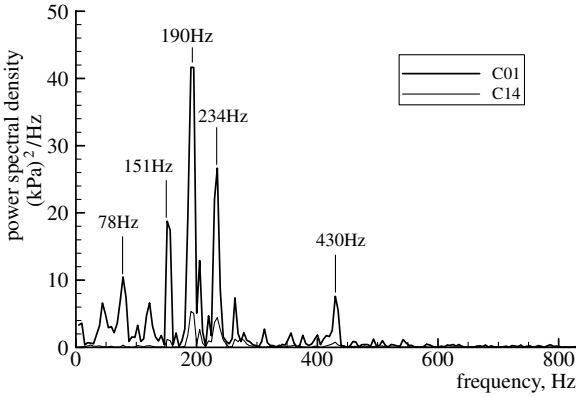

Fig. 8 Spectrum density distributions of typical pressure signals during a little buzz (TR = 50%).

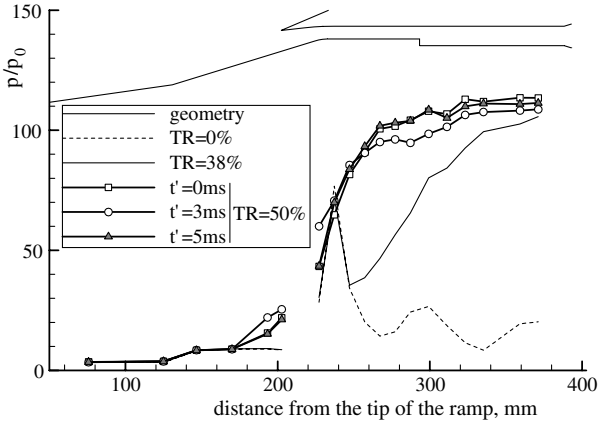

Fig. 9 Instantaneous surface pressure distributions of three typical moments during a little buzz (TR = 50%).

disturbances originated from the separation bubble, which are full of different frequencies, fail to trigger acoustic resonance of the duct.

Figure 9 shows the instantaneous surface pressure distributions of three typical moments ($t' = 0$, $t' = 3$, and $t' = 5$ ms, refer to Fig. 7) during little buzz. The integral time is chosen as 0.2 ms for the calculation of the instantaneous pressure values. The time-averaged surface pressure distributions of TR = 0% and TR = 38% are also shown in Fig. 9 for comparison. At the forepart of the duct, the streamwise pressure gradient is considerably high due to the contributions of three kinds of supersonic pressure-gain processes, namely, the cowl originated shock, the separation bubble induced shock, and the shock train. At the rear part of the isolator and in the combustor, the surface pressure distributions return to a smooth trend because the dominant flow process is supersonic mixing or subsonic diffusing. In general, during little buzz the internal surface pressures

always remain at a high level. But a further analysis reveals that the instantaneous pressure distributions change momentarily. When the separation bubble is small ($t' = 0$ or 5 ms), surface pressures at the entrance of the duct are relatively low, but surface pressures at the rear part of the duct are relatively high, indicating excessive air stored in the duct. When the separation bubble inflates ($t' = 3$ ms), surface pressures at the duct entrance increase as a result of the intensified induced shock, while surface pressures at the rear part of the duct decrease due to the increase of airflow spillage and the resultant reduction of the air stored in the duct.

B. Big Buzz Flow (TR = 58%)

For a further increase of TR to 58%, both the Schlieren movies and the instantaneous surface pressures indicate that the flows of the entire inlet oscillate violently. Figure 10 presents a time slice of typical pressure signals. As compared with signals in Fig. 7, one can notice that the fluctuation amplitudes of current pressure signals are considerably higher. Even the survey point of R04, which is on the second ramp, senses frequent pressure peaks. In addition, the pressure fluctuation intensifies along the flow direction and the amplitude reaches 60 times the freestream pressure at the end of the duct (C14). Figure 10 also shows that the surface pressure oscillations possess some randomicity. For example, the wave trough of the pressure signal of C14 can be as low as 60 times the freestream pressure, but can also reach as high as 90 times the freestream pressure. Furthermore, in a considerably long period (marked by $\Delta t''$) the static pressures of the entire duct remain fairly stable. That is, big buzz at a TR of 58% has certain intermittence in spite of its violent oscillation feature. During the valid experimental process which lasts 5750 ms, the buzz-observed periods sum to 4424 ms. Therefore, the corresponding intermittence factor of buzz is 0.77. Spectrum density distributions of typical pressure signals during big buzz (TR = 58%) are shown in Fig. 11. As shown in this figure, peaks of power spectrum density cluster near 221 Hz, indicating that the fluctuating energy is mainly contained in this narrow frequency region. Also, two peaks can be noticed at 133 and 156 Hz.

The above-mentioned changes of unsteady pressure behaviors suggest significant differences of unsteady flow patterns between big buzz and little buzz. Schlieren pictures and the corresponding surface

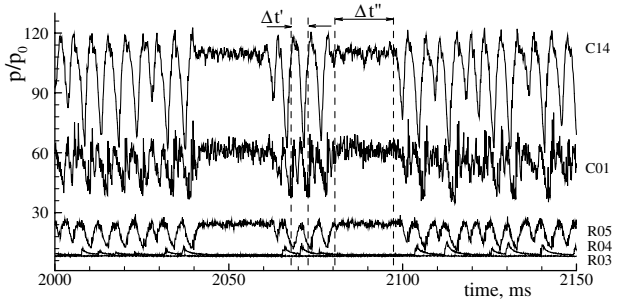

a) Time slice of surface pressure signals

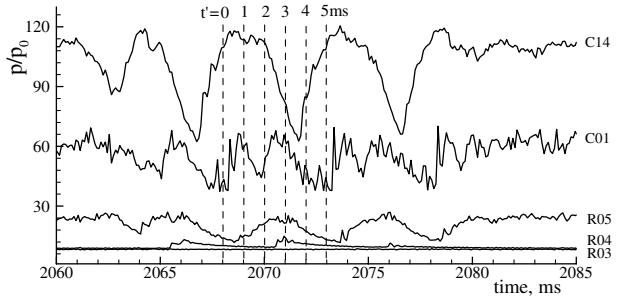

b) Close view of pressure signals in Δt'

Fig. 10 Static pressure-time histories of typical survey points during a big buzz (TR = 58%).

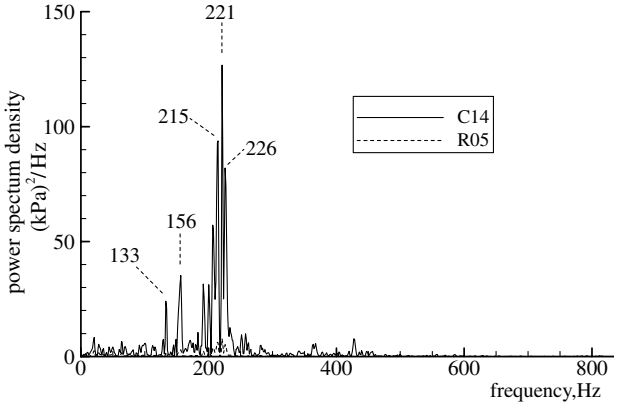

Fig. 11 Spectrum density distributions of typical pressure signals during a big buzz (TR = 58%).

pressure distributions of typical moments (marked in Fig. 10b) in a big buzz cycle are exhibited in Fig. 12 from which the rapid transformations of inlet flow patterns during a buzz cycle can be discussed.

1) $t' = 0$ ms: At this moment, the external compression shock system of the inlet is not influenced and remains at its normal position. The entrance separation bubble formed during the prior buzz cycle has been ingested into the duct and the internal compression shock system is basically established, which can be verified by the consistency of its surface pressure distribution with that of TR = 0%. But small differences still exist in the two surface pressure distributions at the entrance of the duct, indicating the hysteresis effect of the separation bubble. At the aft part of the isolator, an asymmetric shock train with the supersonic core flow deflected to the bottom surface can be observed to originate from the C4 survey point. The shock train leads to a continuous surface pressure ascent in the region of C4–C9 and isolates the transient high pressure (115 times the freestream pressure) in the combustor which resulted from the rapid airflow accumulation.

2) $t' = 1$ ms: Driven by the instantaneous high chamber pressure the shock train moves upstream rapidly and enlarges the high density flow region in the duct to accommodate the increasing stored air. At the same time, a separation bubble appears at the duct entrance and leads to a small quantity of airflow spillage at two sides of the model. The surface pressure distribution at the entrance is thus altered and deviates from that of TR = 0% substantially. The emergence of the separation bubble also brings changes to the shape of the shock train of which the supersonic core flow is presently deflected to the top surface.

3) $t' = 2$ ms: Because of the insufficient exhaust capability of the duct exit, airflow continues accumulating in the duct and the internal high density region expands further. The shock train is thus compressed substantially in the length direction and is confined to the internal flow region upstream of the C4 survey point, leading to a much larger pressure gradient. At the same time, the entrance separation bubble inflates and moves upstream, causing an increased airflow spillage at two sides. Furthermore, the separation induced shock intersects with the cowl originated shock and detaches it from the cowl lip. Therefore, a small quantity of airflow spillage occurs above the cowl.

4) $t' = 3$ ms: Small quantities of airflow spillage above the cowl and at two sides of the entrance still cannot prevent airflow accumulation in the duct. As a result, the separation bubble expands further and causes a serious blockage at the entrance of the inlet. At the same time, the separation induced oblique shock moves upstream continuously until reaching the R4 survey point. The induced shock keeps a constant inclined angle during its movement; thus its top side leaves the cowl lip gradually and the spilled airflow above the cowl increases substantially. From the large inclined angle of the slipping layers which are issued from the shock–shock intersection points, one can infer that a large portion of the coming flow is spilled away from the inlet above the cowl. As a result, the discharged airflow rate

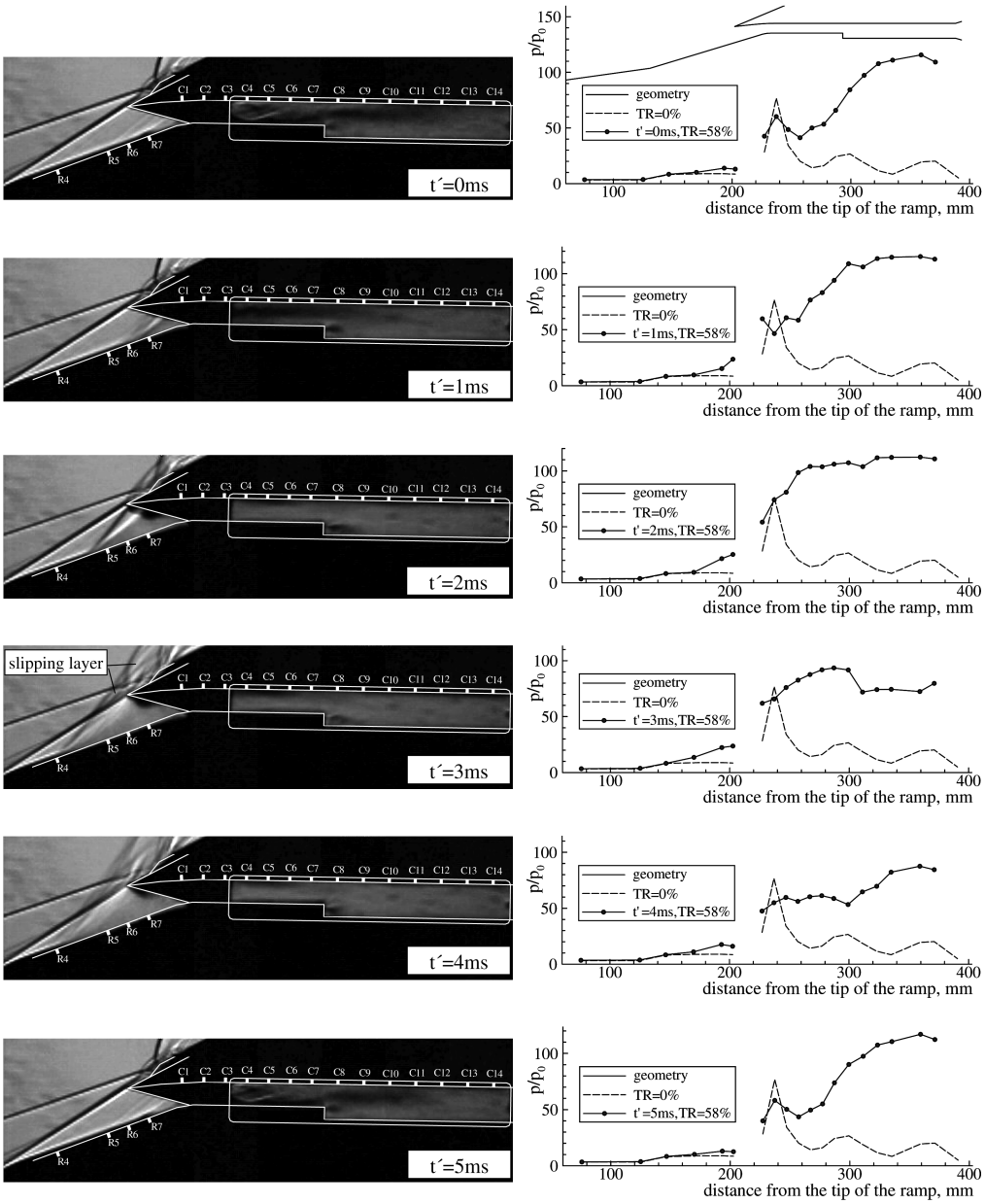

Fig. 12 Schlieren images and the corresponding instantaneous pressure distributions of typical moments in a big buzz cycle (TR = 58%).

of the duct now exceeds the entering airflow rate and the high density air column is emptied gradually. As can be seen, a pressure trough is formed near the exit plug and begins to propagate upstream toward the entrance of the duct.

5) $t' = 4$ ms: The pressure trough reaches the entrance of the inlet and deflates the separation bubble. Simultaneously the separation induced oblique shock begins to move back toward the cowl lip and the entering airflow rate starts to increase. At the aft part of the duct, an increasing high pressure is formed due to the relatively small exhaust airflow rate.

6) $t' = 5$ ms: The separation bubble at the duct entrance shrinks further and finally disappears. The external compression shock system retreats to its normal position and the flow pattern at the duct entrance reestablishes. An asymmetric shock train, which isolates the high pressure in the combustor, appears. That is, a new cycle begins.

From the previous descriptions and discussions, it can be seen that during a big buzz cycle the inlet flow patterns exhibit a series of striking changes. For example, the external compression shock system is first destroyed and then reestablished, the entrance separation bubble is first disgorged and then swallowed, and the shock train in the isolator is first developed and then dispelled. Therefore, the surface pressure fluctuations of big buzz are much more violent than those of little buzz. As compared with traditional supersonic inlet buzz, hypersonic inlet buzz is obviously different in several aspects. First, the transiently expelled unstart shock (i.e., the separation induced shock) is not a normal shock but an oblique one. Both the spilled airflow and the entering airflow are dominantly supersonic flow. Therefore, the motions and the deformations of the external compression shock system during buzz are not controlled by acoustic waves but by the entrance separation bubble. Second, transient supersonic flow exists at the entrance of the duct and at the fore part of the isolator during a buzz cycle; thus, acoustic waves, which play the role of upstream feedback in supersonic inlet buzz, cannot propagate upstream here. Finally, due to the intersection of the unstart shock with the external ramp shock system, two slipping layers are formed but neither enters the duct, thus the slipping layer is not the triggering factor of current hypersonic inlet buzz.

In addition, two instantaneous Schlieren images, which correspond to the start moment and the end moment of $\Delta t''$ (Fig. 10), respectively, are given in Fig. 13 to demonstrate the intermittence of big buzz flow. As expected, the flow patterns of the inlet, including the size of the entrance separation bubble, are temporarily stable during the 17-ms long period.

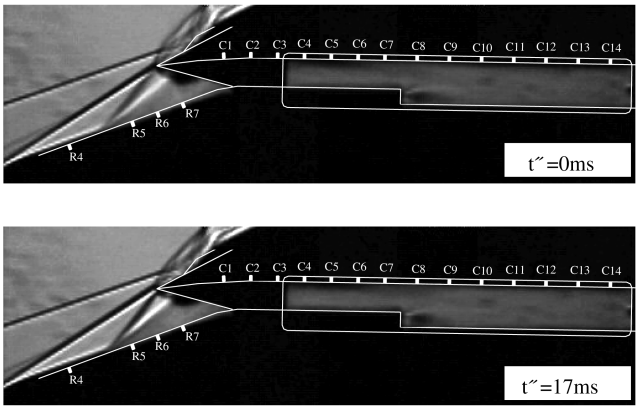

Fig. 13 Schlieren images at the start and the end moments of $\Delta t''$ (TR = 58%).

C. Effects of the Throttling Ratios

Experimental results indicate that when TR is above 58% the inlet always remains at the big buzz state. But the oscillation characteristics vary with the increase of the throttling ratio, as shown in Table 2. When the throttling ratio is increased to 66%, the pressure signal of C14 shows a highly periodic waveform persistently during the entire experimental process which lasts 5500 ms. That is, the intermittence of big buzz vanishes. In general, the change of TR brings no obvious effect on the amplitude of the surface pressure fluctuations, but affects the base frequency of big buzz substantially. As can be seen from Table 2, a 13% increase of the throttling ratio can result in a base frequency augment up to 116 Hz though this trend is not so apparent at a higher throttling ratio (above 71%). Figure 14 presents the pressure-time histories of C14 at TRs of 58 and 85%. One can notice that the discrepancy of the two waveforms is pronounced for the width of wave crests but small for the width of wave troughs. Therefore, it can be inferred that the influence of the throttling ratio on buzz frequency is exerted mainly by its impact on the internal air accumulation process rather than on the external shock system motion. This deduction is consistent with the observations of Schlieren videos. At different throttling ratios, the Schlieren images which record the expelled shock system all sum to three frames per buzz cycle according to the statistical calculations. That is, the external shock system motions all take up 1.5–2.0 ms with a consideration of the sampling rate of 2000 frames per second. In addition, at a higher throttling ratio the waveform of the pressure signal is more regular and the corresponding power spectrum density becomes more concentrative (Fig. 15).

The throttling ratios are also found to have significant impacts on the flow patterns of big buzz. A combined analysis of the instantaneous pressure distributions with the Schlieren movies indicates that when the throttling ratio is increased to and above 71%, the airflow both at the duct entrance and in the isolator is entirely reversed. Figure 16 exhibits an instantaneous Schlieren image which is recorded at a TR of 71%. As clearly shown in this figure, the supersonic expansion region behind the backstep disappears. Instead a density-gradual-change region appears above the backstep corner (marked by a circled 1 in Fig. 16). The position and the shape of this abnormal region all exhibit the characteristics of a subsonic front step flow, suggesting the occupation of reversed flow at the aft part of the isolator. Furthermore, a slight discontinuity of the density distribution, which is vertical to the local flow direction, appears at

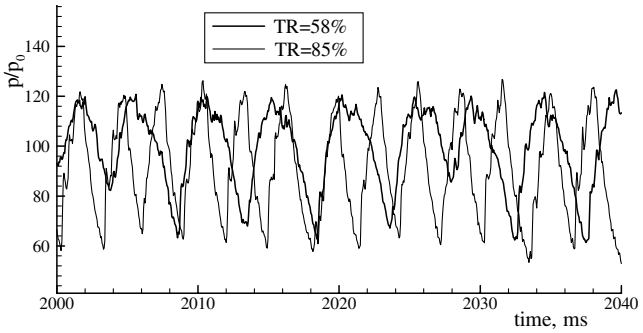

Fig. 14 Pressure signals of C14 at different throttling ratios.

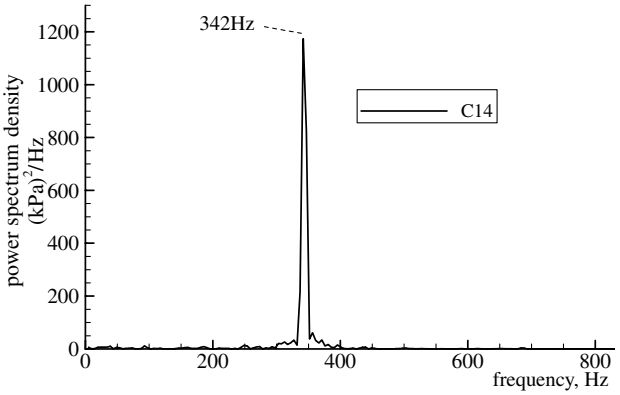

Fig. 15 Spectrum density distribution of the pressure signal of C14 during a big buzz (TR = 58%).

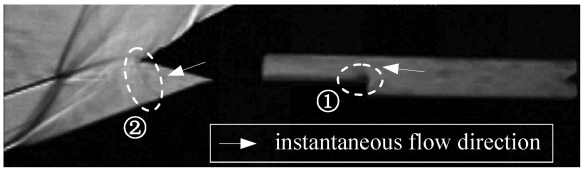

Fig. 16 Transient reversed flows in the isolator and at the duct entrance during a big buzz (TR = 71%).

the entrance plane of the duct (marked by a circled 2 in Fig. 16). With the aid of numerical simulations, a plausible explanation of the discontinuity is obtained as follows: the entrance part of the inlet acts as a diverging duct because the local flow is temporarily reversed, and thus the internal subsonic flow is accelerated here to a low supersonic speed and is slightly overexpanded. Consequently, a weak normal shock appears for the need of pressure balance with the coming flow. As to the oscillation scopes of the external shock system and the internal shock train, they are also substantially affected by the throttling ratio variations. Figure 17 displays two typical Schlieren images which are recorded at a TR of 85%. As can be inferred from the inclined angle of the expelled shock and verified by the substantial pressure fluctuations of R1, the external shock system is found to reach the fore part of the first ramp surface. The internal shock train moves downstream until it comes to the C9 survey point, due to the instantaneous low pressure in the duct.

Table 2 Oscillation characteristics of a big buzz at different throttling ratios

Throttling ratio	58%	66%	71%	85%
Base frequency	221	296	337	342
Typical wave trough value of pressure-time history of C14 ($/p_0$)	70	63	61	56
Typical wave crest value of pressure-time history of C14 ($/p_0$)	118	119	123	123
Duration of the shock-disgorged period, ms	1.5–2.0	1.5–2.0	1.5–2.0	1.5–2.0
The most downstream position of the shock train during its oscillatory motions	C4	C4	C6	C9

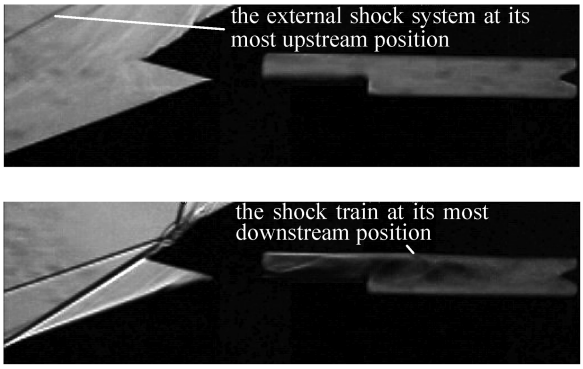

Fig. 17 Utmost positions of the external and internal shock motions in a big buzz cycle (TR = 58%).

D. Mechanism Analysis of Hypersonic Inlet Buzz

In principle, the establishment of a feedback loop is the necessary condition of self-excited flows [21]. For the specific phenomenon of inlet buzz, the feedback loop can be constructed as follows: instability waves with certain amplitude are generated at or before the entrance of the duct, then the waves are convected downstream with the stream and are maintained or amplified there, and finally the downstream waves propagate back to the upstream source of the instability waves by certain means. As to the traditional supersonic inlet buzz, there always stands a subcritical normal shock before the duct entrance; therefore the shock-induced boundary layer separation or the slipping layer issued from the shock–shock intersection point can be the upstream instability source. The impingements of the convected vortical waves on the cowl, on the ramp, and on the exit throat surface often generate the feedback signals. Because in the major region (downstream of the subcritical normal shock) and for the most time the buzz flow is subsonic, the downstream generated acoustic waves can propagate upstream easily. As a result, acoustic waves often play an important role in the feedback loop of supersonic inlet buzz. Therefore, the base frequency and other energy-containing frequencies of supersonic inlet buzz are closely related to the acoustic resonance modes of the duct.

However, according to current and previous experimental results (Table 3), the fundamental frequency and other peak frequencies of hypersonic inlet buzz show little relation with the acoustic resonance modes of the ducts, but substantially depend on the exit throttling ratios. The former conclusion is understandable in consideration of the existence of the temporary supersonic flow region which impedes the upstream propagation of acoustic waves and leads to the invalidation of the traditional supersonic inlet buzz mechanism. The latter conclusion, or the close relation of the base frequency with the exit throttling ratio, indicates that the discrepancy of the capture capability and the exhaust capability of airflow may be a driving element of hypersonic inlet buzz. Take, for example, TR = 58%. The maximum exhaust capability of airflow at the duct exit is estimated to be 0.15 kg/s according to the highest sustainable chamber pressure (refer to Fig. 12), the total temperature of the coming flow, and the exit throat area. While the airflow capture capability of the inlet at a started condition is 0.18 kg/s, the imbalance of the airflow rate is serious and must be compensated by the entrance spillage. Taking the airflow spillage at the duct entrance as the upstream instability source, one can analyze the feedback loop of the hypersonic inlet buzz as follows: decrease of the entrance spillage → accumulation of airflow in the duct → increase of the chamber pressure → the upstream movement of the internal shock train driven by the high chamber pressure → appearance, expansion, and upstream movement of the entrance separation bubble → increase of the entrance spillage; increase of the entrance spillage → gradual drainage of the compressed air stored in the duct (possible through two ends of the duct) → decrease of the chamber pressure → upstream propagation of the low pressure waves through a low speed flow region such as separation bubble, boundary layer, etc. → shrinkage and downstream movement of the entrance separation bubble → decrease of the inlet spillage. As can be seen, the response of the duct flow always makes a negative feedback to the entrance spillage variation. It seems that the airflow spilling process will always take place in a steady manner. But, in fact, at certain conditions the spilling process may develop into an oscillatory motion due to the feedback delay which forms a phase lag between the original disturbance and the response. According to current experimental results, when the maximum exhaust capability of airflow is less than the theoretical capture capability of airflow by 5.5% or less, the spillage takes place at two sides of the entrance steadily. But when the difference ratio is increased to or above 11.7%, additional transient spillage occurs above the cowl and triggers little buzz. Violent big buzz arises when the difference ratio is increased to or above 16.7%.

It is apparent that the delay time of the negative feedback determines the cycle length and the base frequency of the hypersonic inlet buzz. Because the response mechanism of the spillage-increase disturbance is different from that of the spillage-decrease disturbance, the delay time will be discussed, respectively. For simplification, the analysis is made while the external shock system of the inlet is slightly upstream of its normal position. For one case, if the entrance spillage increases, that is, the external shock system moves away from its original position and shifts toward the ramp tip, the subsequent decrease of the entrance spillage will occur at the moment when the external shock system moves back from the upstream direction. That is, the delay time of the negative feedback is equal to the duration of the external shock expelling and retreating process. As stated above, the duration of the external shock motion is basically independent of the throttling ratios and equals 1.5–2.0 ms though its scope is closely related to the throttling ratios. For another case, if the entrance spillage decreases, that is, the external shock system moves close to the cowl lip, the subsequent increase of the inlet spillage will occur at the moment when the entrance shock system is expelled. In other words, the delay time of the negative feedback is equal to the duration of the mass filling-up process of the duct. Obviously, the required time of the mass filling-up process is related to the duct volume, the maximum sustainable density of the stored air column, and the difference between the entering airflow rate and the exhaust airflow rate. For a specific inlet model and given test conditions, the duct volume, the maximum air density, and the entering airflow rate are all fixed; therefore the mass filling-up time is decided by the exhaust airflow rate which is subject to the exit throttling ratio. Take the example for the condition of TR = 58% again. The duct volume is 1.66×10^{-4} m^3, and the maximum density of the stored air column is estimated to be 1.11 kg/m^3 according to the maximum sustainable duct pressure (refer to Fig. 12, $t' = 2$ ms) and the total temperature of the coming flow. As a result,

Table 3 Base frequencies of a hypersonic inlet buzz obtained by different experiments

	Current results	Tan and Guo [4]	Rodi et al. [19]	Hawkins and Marquart [22]
Freestream Mach no.	4.92	6.0	4.03	5.0
Duct length, m	0.19	1.27	0.71	1.47
Typical sound speed, m/s	461	799	343.8	340[a]
Average duct Mach no.	0.4	0.4	0.4[a]	0.4[a]
Base frequency of acoustic resonance mode, Hz	510	132	103	49
Experimentally obtained base frequency, Hz	190–342	8–23	300	150–180

[a]An accurate value is not stated in the original paper. A typical value is assumed.

Table 4 Comparison of the predicted and the experimentally obtained base frequencies of a big buzz at different throttling ratios

Throttling ratio	58%	66%	71%	85%
Estimated mass filling-up time, ms	2.50	1.42	1.11	0.71
Predicted base frequency, Hz	222–250	293–343	322–383	369–452
Experimentally obtained base frequency, Hz	221	296	337	342

the maximum stored air in the duct is calculated to be 1.84×10^{-4} kg. The airflow rate difference is already known as 0.03 kg/s. If one neglects the residual air in the duct, the mass filling-up time ought to be 6.13 ms. Therefore, the duration of a big buzz cycle is 7.63–8.13 ms and the corresponding base frequency is 123–131 Hz. The predicted value is remarkably different from the experimentally observed value of 221 Hz. This discrepancy is possibly caused by the usage of the maximum exhaust airflow rate rather than the average one and by the neglect of the residual air in the duct. Taking a 50% prefilling degree of the duct and a 95% average ratio of the maximum exhaust airflow rate, the base frequencies of the hypersonic inlet buzz at different throttling ratios are recalculated according to the following formula:

$$f_0 = \left(t_{\text{shock}} + \frac{m_{\text{stored}} \cdot (1 - r_{\text{prefill}})}{q_{\text{capture}} - q_{\text{exhaust}} \cdot r_{\text{average}}} \right)^{-1}$$

where t_{shock} denotes the external shock motion time, m_{stored} the maximum stored air mass, q_{capture} the capture airflow rate, q_{exhaust} the maximum exhaust airflow rate, r_{prefill} the prefilling ratio, and r_{average} the average ratio. The results are listed in Table 4. It can be said from Table 4 that the predicted base frequencies agree well with the experimental results both in trends and in values, which verifies the validity of the newly proposed mechanism of the hypersonic inlet buzz.

VII. Conclusions

An experimental study of a rectangular hypersonic inlet has been performed at a freestream Mach number of 5.0 to achieve a better understanding of hypersonic inlet buzz, including the oscillation characteristics, the unsteady flow patterns, and the oscillation mechanism. During the tests, a throttling device, attached to the rear of the test model, is used to increase the inlet backpressure until unstart occurs. With the aid of time-resolved Schlieren and fast response pressure measurements, the unsteady flow patterns and the unsteady surface pressures during buzz are obtained at different throttling ratios. As observed in the present experiments, the unstarted flows can be classified into two distinct types: little buzz and big buzz. During a little buzz cycle, a large separation bubble appears at the duct entrance and shrinks and expands periodically, resulting in an oscillatory motion of the induced oblique shock wave. The inlet flow patterns exhibit a series of striking changes during a big buzz cycle. For example, the external compression shock system is first destroyed and then reestablished, the entrance separation bubble is first disgorged and then swallowed, and the shock train in the isolator is first developed and then dispelled. In addition, during a big buzz cycle transient reversed flow may occur at the duct entrance and in the isolator. The throttling ratio is found to substantially affect the base frequency of big buzz in spite of its unapparent impacts on the amplitude of pressure fluctuations. In the present experiments, a 13% increase of the throttling ratio can result in a base frequency augment up to 116 Hz.

Because of the presence of a large transient supersonic region in the duct for both types of buzz flows, the upstream propagation of acoustic waves is impeded temporarily. As a result the oscillation mechanism of conventional supersonic inlets based on the acoustic resonance cannot serve as the theoretical background for the hypersonic inlet buzz. Therefore a new buzz mechanism is brought forward in which the airflow spillage at the duct entrance is taken as the disturbing source and three communicating ways, namely, convection, shock train motion, and acoustic wave propagation, jointly establish the signal feedback loop. According to the newly developed oscillation mechanism, the base frequencies of hypersonic inlet buzz at different throttling ratios are estimated and found in good consistency with current experimental results.

Acknowledgment

This work is supported by the National Nature Science Foundation of the People's Republic of China through Grant No. 50606017.

References

[1] Voland, R. T., Auslender, A. H., and Smart, M. K., "CIAM/NASA Mach 6.5 Scramjet Flight and Ground Test," AIAA Paper 1999-4848, 1999.

[2] Curran, E. T., and Murthy, S. N. B., *Scramjet Propulsion, Progress in Astronautics and Aeronautics*, Vol. 189, AIAA, Reston, VA, 2001, pp. 462–466.

[3] McClinton, C. R., and Hunt, J. L., "Airbreathing Hypersonic Technology Vision Vehicles and Development Dreams," AIAA 1999-4987, 1999.

[4] Tan, H. J., and Guo, R. W., "Experimental Study of the Unstable-Unstarted Condition of a Hypersonic Inlet at Mach 6," *Journal of Propulsion and Power*, Vol. 23, No. 4, 2007, pp. 783–788. doi:10.2514/1.28039

[5] Oswatitsch, K., "Der Druckrückgewinn bei Geschossen mit Rückstossantrieb bei hohen Übershallgeschwindigkeiten (Der Wirkungsgrad vos Stossdiffusoren)," Bericht Nr. 1005 Forsch. und Entwickl. des Heereswaffenamtes (Göttingen), 1944; also "Pressure Recovery for Missiles with Reaction Propulsion at High Supersonic Speeds," NACA Translation TM 1140, 1944 (in English).

[6] Ferri, A., and Nucci, L. M., "The Origin of Aerodynamic Instability of Supersonic Inlets at Subcritical Conditions," NACA RM L50K30, 1951.

[7] Dailey, C. L., "Supersonic Diffuser Instability," Ph.D. Thesis, California Institute of Technology, Pasadena, CA, 1954.

[8] Fisher, S. A., Neale, M. C., and Brooks, A. J., "On the Sub-Critical Stability of Variable Ramp Intakes at Mach Numbers Around 2," National Gas Turbine Establishment Rept. ARC-R/M-3711, Feb. 1970.

[9] Sajben, M., Bogar, T. J., and Kroutil, J. C., "Experimental Study of Flows in a Two-Dimensional Inlet Model," AIAA Paper 83-0176, Jan. 1983.

[10] Newsome, R. W., "Numerical Simulation of Near-Critical and Unsteady, Subcritical Inlet Flow," *AIAA Journal*, Vol. 22, No. 10, 1984, pp. 1375–1379. doi:10.2514/3.48577

[11] Lu, P. J., and Jain, L. T., "Numerical Investigation of Inlet Buzz Flow," *Journal of Propulsion and Power*, Vol. 14, No. 1, 1998, pp. 90–100. doi:10.2514/2.5254

[12] Trapier, S., Duveau, P., and Deck, S., "Experimental Study of Supersonic Inlet Buzz," *AIAA Journal*, Vol. 44, No. 10, 2006, pp. 2354–2365. doi:10.2514/1.20451

[13] Trapier, S., Deck, S., and Duveau, P., "Time-Frequency Analysis and Detection of Supersonic Inlet Buzz," *AIAA Journal*, Vol. 45, No. 9, 2007, pp. 2273–2284. doi:10.2514/1.29196

[14] Hirschen, C., Herrmann, D., and Gülhan, A., "Experimental Investigations of the Performance and Unsteady Behavior of a Supersonic Intake," *Journal of Propulsion and Power*, Vol. 23, No. 3, 2007, pp. 566–574. doi:10.2514/1.25103

[15] Scott, D. H., "Wind-Tunnel Blockage and Actuation Systems Test of a Two-Dimensional Scramjet Inlet Unstart Model at Mach 6," NASA TM-109152, 1994.

[16] Bao, W., Chang, J. T., Guo, X. G., and Cui, T., "Unstart Simulation of Scramjet Inlets," *Journal of Aerospace Power*, Vol. 20, No. 5, 2005, pp. 731–735.

[17] Yuan, H. C., and Liang, D. W., "Characteristic Analysis of Unstart Performance for Hypersonic Side-Wall Inlet Model," *Journal of Nanjing University of Aeronautics & Astronautics*, Vol. 36, No. 3, 2004, pp. 683–687.

[18] Sun, S., Zhang, H. Y., Cheng, K. M., and Wu, Y. Z., "The Full Flowpath Analysis of a Hypersonic Vehicle," *Chinese Journal of Aeronautics*, Vol. 20, No. 5, 2007, pp. 385–393. doi:10.1016/S1000-9361(07)60059-4

[19] Rodi, P. E., Emamit, S., and Trexlers, C. A., "Unsteady Pressure Behavior in a Ramjet/Scramjet Inlet," *Journal of Propulsion and Power*, Vol. 12, No. 3, 1996, pp. 486–493. doi:10.2514/3.24061

[20] Wang, C. P., Cheng, K. M., Wang, J. F., and Wu, Y. Z., "Flow Field Calibrations and Force Tests of an AGARD Model in a Hypersonic Wind Tunnel of NUAA," *Proceedings of the China 1st Modern Aerodynamics & Aerothermodynamics Conference*, China Aerodynamics Research Society, Beijing, 2006, pp. 356–361.

[21] Meire, G. E., Szumowski, A. P., and Selerowicz, W. C., "Self-Excited Oscillations in Internal Transonic Flows," *Progress of Aerospace Sciences*, Vol. 27, No. 2, 1990, pp. 145–200.

[22] Hawkins, W. R., and Marquart, E. J., "Two-Dimensional Generic Inlet Unstart Detection at Mach 2.5-5.0," AIAA Paper 95-6019, April 1995.

R. Bowersox
Associate Editor